Arch. Metall. Mater. **63** (2018), 4, 1755-1761

DOI: 10.24425/amm.2018.125102

C. PANDEY*[#], M. MOHAN MAHAPATRA**, P. KUMAR****, P. KUMAR***, J.G. THAKARE****

# CHARACTERIZATION OF WELD FUSION ZONE FOR TIG WELDED P91 AND P92 STEELS

The welding of nuclear grade P91 and P92 steel plate of thickness 5.2 mm were performed using the autogenous tungsten inert gas (TIG) welding process. The welded joint of P91 and P92 steel plate were subjected to the varying post weld heat-treatment (PWHT) including the post weld heat treatment (PWHT) and re-austenitizing based tempering (PWNT). A comparative study was performed related to the microstructure evolution in fusion zone (FZ) of both the welded joint using the scanning electron microscope and optical microscope in a different condition of heat treatment. The hardness test of the FZ for both joints was also conducted in a different condition of heat treatment. P92 steel welded joint have observed the higher tendency of the $\delta$ ferrite formation that led to the great variation in hardness of the P92 FZ. The homogeneous microstructure (absence of $\delta$ ferrite) and acceptable hardness was observed after the PWNT treatment for both the welded joint.

*Keywords:* P91; P92; fusion zone; microstructure; TIG

## 1. Introduction

The nuclear grade steel is well known for high-temperature application in a range of 600-650°C due to their thermo-physical properties and creep rupture strength [1,2]. The P91 and P92 steel are mostly used in the newly developed nuclear power plants and maintenance of the old power plants to enhance the efficiency of power plants and simultaneously reduction in the emission of the greenhouse gases [3]. The steel application becomes more attractive due to its high-temperature microstructure stability for a prolonged time and weldability [4]. Both the steels offer almost similar microstructure of tempered martensite. The microstructure stability of steel derived from the precipitation hardening [5,6]. In both the steel, Cr is used as the primary alloying elements. The addition of Mo and W is carried out to enhance the solid solution hardening of the steels. In P91 steel, the higher weight percentage of Mo about 0.95% is used, however, W about 1.80% is used in P92 steel [7]. The other alloying element percentage remain same in both the steel except the addition of B in P92 steel about 0.001% [5]. The B addition in P92 steel makes it superior to the P91 steel by enhancing the creep strength of it. The improved creep strength is attributed to the formation of Cr and B-rich $M_{23}C_6$ type carbide precipitates that reduces the coarsening rate of the Cr-rich $M_{23}C_6$ [8,9].

In general, the P91 and P92 steel can be welded easily by the arc welding process and shows the good weldability [10,11]. However, the creep rupture strength of the welded joint makes a serious issue of their weldability. The welded joint of both steel offers the poor creep rupture strength as compared to the virgin base metal as a result of the formation of the soft inter-critical heat affected zone (ICHAZ) that leads to the premature Type IV failure of the welded joint [12-14]. The failure of the P91 and P92 steel welded joint from the boundary of base and heat affected zone is referred as the Type IV cracking. The Type IV failure in welded joint is associated with the heterogeneous microstructure that results of rapid heating and cooling weld cycle. The formation of the $\delta$ ferrite in the fusion zone (FZ) also reduces the creep strength and mechanical properties of the welded joints. However, the P92 steel shows a higher propensity to the formation of the $\delta$ ferrite patches due to the higher weight percentage of ferrite stabilizer [15,16]. The post weld heat treatment (PWHT) is suggested to reduce the microstructure heterogeneity across the welded joint, impart ductility and softening of the martensite. However, it was concluded that the tendency of the type IV cracking can be minimized but it cannot be removed completely using the post weld heat treatment process [12,17,18].

In present work, two different type of the post weld heat treatment was utilized for the tungsten inert gas welded P91 and P92 steel welded joint and studied their effect on the microstructure homogeneity. The formation of the $\delta$ ferrite FZ and the effect of the heat treatment on it was also performed.

## 2. Experimental details

The steel plates of P91 and P92 steel were received in normalized and tempered condition. The plates of dimension 100 mm×75 mm×5.2 mm were used for the joining purpose.

* DEPARTMENT OF MECHANICAL ENGINEERING, SRM IST DELHI NCR CAMPUS MODINAGAR UTTAR PRADESH 201204, INDIA
** INDIAN INSTITUTE OF TECHNOLOGY, SCHOOL OF MECHANICAL SCIENCES, BHUBANESWAR, ODISHA 751013, INDIA
*** BIRLA INSTITUTE OF TECHNOLOGY, DEPARTMENT OF PRODUCTION ENGINEERING, MESRA RANCHI (INDIA)-835 215
**** INDIAN INSTITUTE OF TECHNOLOGY ROORKEE, DEPARTMENT OF MECHANICAL AND INDUSTRIAL ENGINEERINGUTTRAKHAND-247667, INDIA

[#] Corresponding author: chandanpy.1989@gmail.com

The plates are welded using the autogenous tungsten inert gas (TIG) process. The welding process parameters are depicted in Table 1. Eq. 1 [19] was used to calculate the heat input (KJ/mm) during welding process.

$$Q(\text{KJ/mm}) = \frac{V \text{X} I \text{X} \eta \text{X} 60}{T} \quad (1)$$

Where $V$ = arc voltage, $I$ = welding current, $T$ = travel speed (mm/min), and $\eta$ is arc efficiency taken as 0.90 in present work.

TABLE 1

Summary of welding process used in weld preparation

| Parameters | TIG Process |
|---|---|
| Electrode | EW-2%Th |
| Electrode tip angle | 60° |
| Polarity | DCEN, water cooled torch |
| Shielding gas | Commercially pure argon (99.9%) |
| Weld groove | No |
| Arc gap | 3 mm |
| Arc voltage (V) | 14-15 |
| Travel speed (mm/min | 80 |
| Welding current (amp) | 220 |
| Avg. heat input | 2.50 kJ/mm |

The composition of the plates is depicted in Table 2. The preheating of the plates was conducted at 250°C before the welding. After the welding plates were subjected to tempering at 760°C for 2 h, followed by air cooling (PWDT), and re-austenitization at 1040°C for 40 min followed by air cooling+ tempering at 760° for 2 h, followed by air cooling (PWNT). The schematic of the heat treatment is shown in Fig. 1. For multi-pass

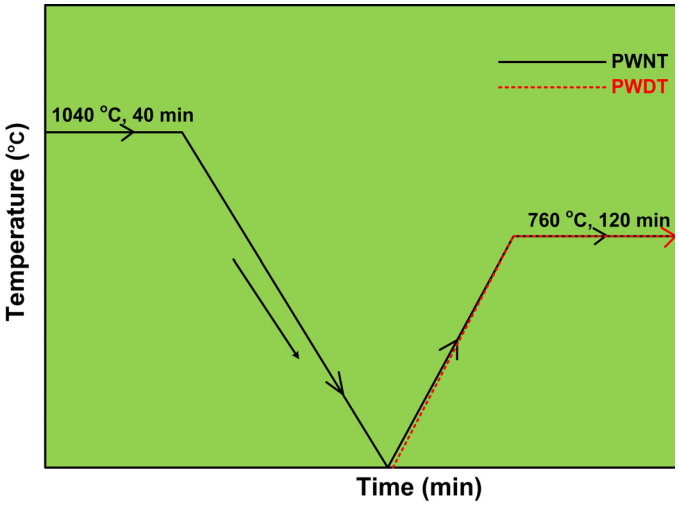


Fig. 1. Schematic of the heat treatment performed on the welded joint

TIG and SMAW welding process, to achieve the homogeneous microstructure across the welded joint similar heat treatment was also performed by Pandey et al. [20,21].

The welded joints cut in the transverse direction and subjected to a standard metallographic technique including grinding, paper polishing and cloth polishing with alumina powder. The polished sample were etched in a mixed solution of 100 ml ethanol, 5 ml HCL, and 1g picric acid (Vilella's solution). The polished and etched welded samples were characterized using the field emission scanning electron microscope, optical microscope, and hardness testing.

## 3. Results and discussion

### 3.1. As-received material

The microstructure of the P91 and P92 steel shows the similar microstructural behavior having tempered martensite with transgranular and intergranular precipitates. The coarsened $M_{23}C_6$ precipitates are observed along the intergranular region while fine MX and $M_{23}C_6$ particles inside the transgranular region. The microstructural stability derived from the precipitates. The precipitates enhance the microstructural stability during the prolonged period by impeding the movement of subgrain boundaries, lath widening and impeding the movement of dislocations. The transgranular precipitates show higher coarsening rate as compared to intergranular precipitates during the creep exposure. In P92 steel the addition of B reduces the coarsening rate of the transgranular precipitates and enhance the creep strength of the material [22]. The micrograph of the P91 and P92 steel is shown in Fig. 2a-d. The schematic evolution of the precipitates along the grain boundaries, lath packets and lath blocks is shown in Fig. 2e [23].

### 3.2. Microstructure of the fusion zone

The micrograph of FZ is shown in Fig. 3 for both P91 and P92 steel welded joint. For P91 steel welded joint, FZ is characterized with lath blocks and packets. The untempered martensite is arrested with the prior austenite grains (PAGs). Fig. 3b shows the parallel prior austenite grain boundaries (PAGBs) in the FZ. In P91 steel welded joint, the $\delta$ ferrite is not observed that is attributed to the absence of low ferrite stabilizer in P91 steel. The FZ of P92 steel reveals the presence of $\delta$ ferrite having different morphology. Within the PAGBs, the lath blocks of different orientation are observed inside the lath packets while the

TABLE 2

Chemical composition of P91 and P92 steel (wt. %)

| Element | Chemical composition (wt. %) | | | | | | | | | | | | |
|---|---|---|---|---|---|---|---|---|---|---|---|---|---|
| | C | Mn | Cr | Si | Mo | V | Nb | Ni | S | Ti | W | Cu | Fe |
| P91 steel | 0.12 | 0.54 | 8.48 | 0.28 | 0.95 | 0.18 | 0.05 | 0.35 | 0.011 | 0.012 | <0.001 | 0.06 | Rest |
| P92 steel | 0.11 | 0.58 | 9.09 | 0.48 | 0.42 | 0.24 | 0.05 | 0.30 | 0.003 | 0.002 | 1.87 | 0.03 | Rest |

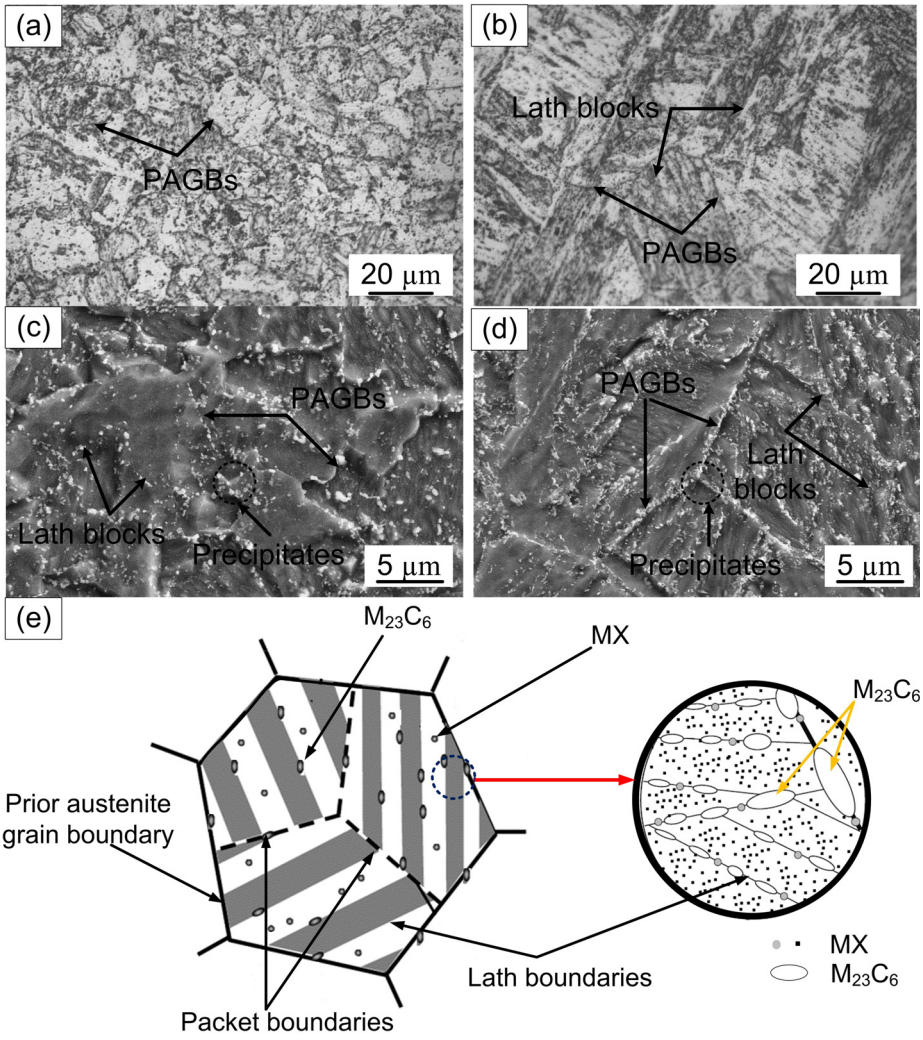


Fig. 2. Optical micrograph of as-received (a) P91 steel, (b) P92 steel; SEM micrograph for (c) P91 steel, (d) P92 steel, (e) schematic evolution of micrograph in P91 and P92 steel

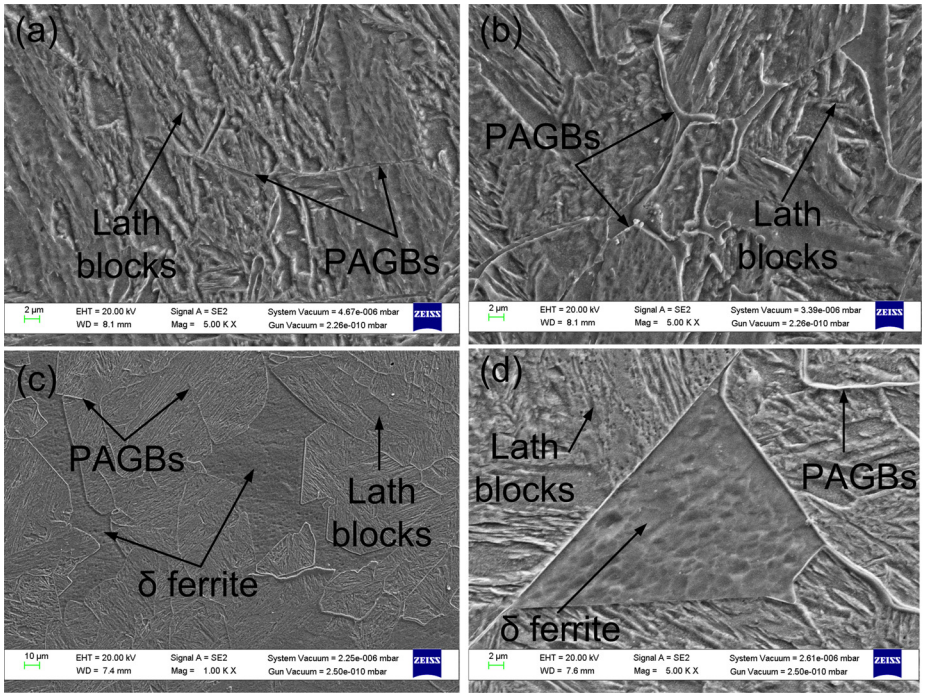


Fig. 3. Micrograph of P91 FZ (a) and (b), respectively; micrograph of P92 FZ (c) and (d), respectively

$\delta$ ferrite region shows the absence of lath morphology, as shown in Fig. 3c. To confirm the absence of the lath morphology inside the $\delta$ ferrite region, higher magnification micrograph is shown in Fig. 3d. In P92 steel welds, the higher weight percentage of the ferrite stabilizer is responsible for the formation of the $\delta$ ferrite.

The optical micrograph has also been taken at a different region of the FZ for both the weld joint. In P91 steel welded joint, typical untempered columnar laths of different orientation are observed, as shown in Fig. 4a. However, at a different location, a patch of $\delta$ ferrite is observed that results from the wide solidification and higher heat input due to a single pass. The similar observation has also been reported by Pandey et al. [15] for dissimilar weld joint of P91 and P92 steel. The FZ of P92 steel welded joint shows the ferrite patches clearly. The size of ferrite zone varies from region to region. The bigger $\delta$ ferrite region in FZ is shown in Fig. 4b. The formation of the high volume fraction of the $\delta$ ferrite in P92 steel FZ might be due to wide solidification, higher heat input, and presence of higher amount of ferrite stabilizer. The FZ is further characterized after the post weld heat treatment (PWHT).

After the PWHT, martensite softening and precipitate evolution occur both in the intergranular and transgranular region. Fig. 5a-b shows the micrograph of P91 weld fusion zone after the PWHT. At such high magnification, the visibility of $\delta$ ferrite is not clear. The micrograph shows the lath blocks and PAGBs with precipitates along it. The fine precipitates along the lath blocks and inside the matrix region is observed in Fig. 5b. For P92 welds, the FZ still shows the presence of ferrite patches that is free from the lath morphology and carbide precipitates, as shown in Fig. 5c. The PAGBS and lath blocks and $\delta$ ferrite boundaries get decorated with the Cr, Fe, Mo and W-rich $M_{23}C_6$ precipitate. The precipitates along the $\delta$ ferrite boundaries and the carbide precipitate free $\delta$ ferrite region are shown in Fig. 5d. The optical micrograph of FZ shows the presence of $\delta$ ferrite for both welded joint. However, in P91 steel welds, FZ shows the fewer amount of ferrite patches as compared to P92 steel welds. The precipitates along the PAGBs are clearly observed in optical micrograph in black dotted form. In P91 steel welded joint, FZ also shows the columnar lath morphology, as shown in Fig. 5e. For more confirmation of the presence of $\delta$ ferrite, the optical micrograph of FZ for both the joints has been taken at a different location, as shown in Fig. 6.

At a low magnification of 200×, a number of $\delta$ ferrite patches has been observed in FZ of P91 welded joint (Fig. 6a). At some other location of FZ, $\delta$ ferrite patches are observed, as shown in Fig. 6b-c. The size of $\delta$ ferrite patches is observed lower as compared to FZ of P92 welded joint. The number density and size of ferrite patches in FZ of P92 welded joint at low magnification (200×) are observed higher as compared to P91 steel welded joint, as shown in Fig. 6d. The bigger size of ferrite zone in FZ of P92 welded joint is also confirmed from the Fig. 6e,f, respectively. In P92 FZ, beyond the different shape and morphology, some elongated shape $\delta$ ferrite patches are also noticed in Fig. 6e.

The PWNT treatment deals with the re-austenitizing based tempering of welded joint. The re-austenitizing of the welded joint results in austenitizing of the welded joint and dissolution of fine $M_{23}C_6$ precipitates and $\delta$ ferrite. The tempering of the re-austenitized welded joint impart the ductility and softening of the martensite. It also results in the evolution of the precipitates. The micrograph of FZ for both the welded joint after the PWNT treatment is shown in Fig. 7. Some coarse precipitates are clearly observed in optical micrograph for both the welded joint. In P91 FZ, the number density of coarse $M_{23}C_6$ precipitates is observed higher as compared to P92 FZ. During the re-austenitizing (normalizing), some fine precipitates get dissolved however, the

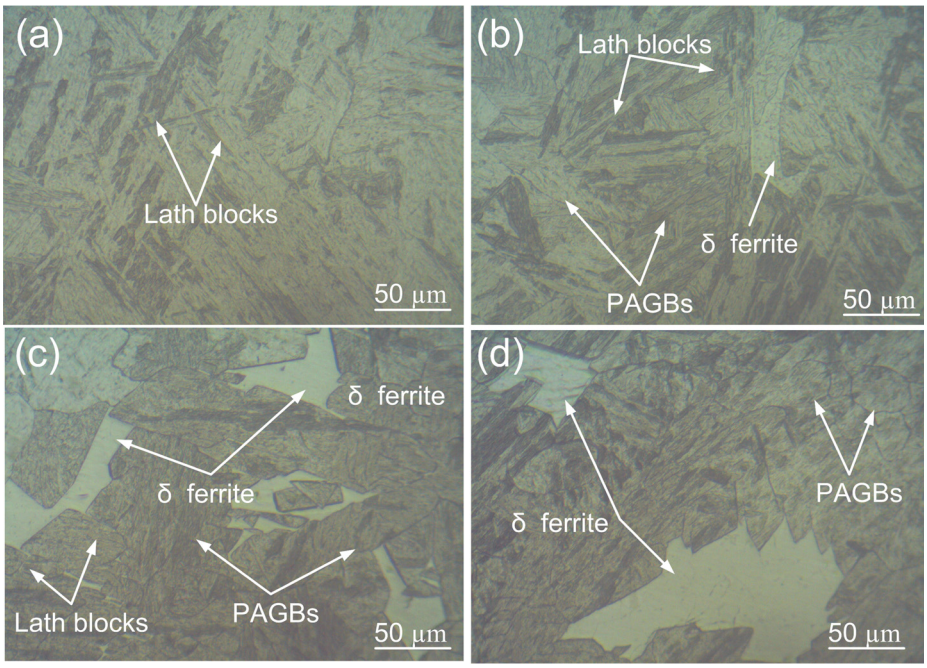


Fig. 4. Optical micrograph of P91 FZ (a) and (b), respectively; micrograph of P92 FZ (c) and (d), respectively

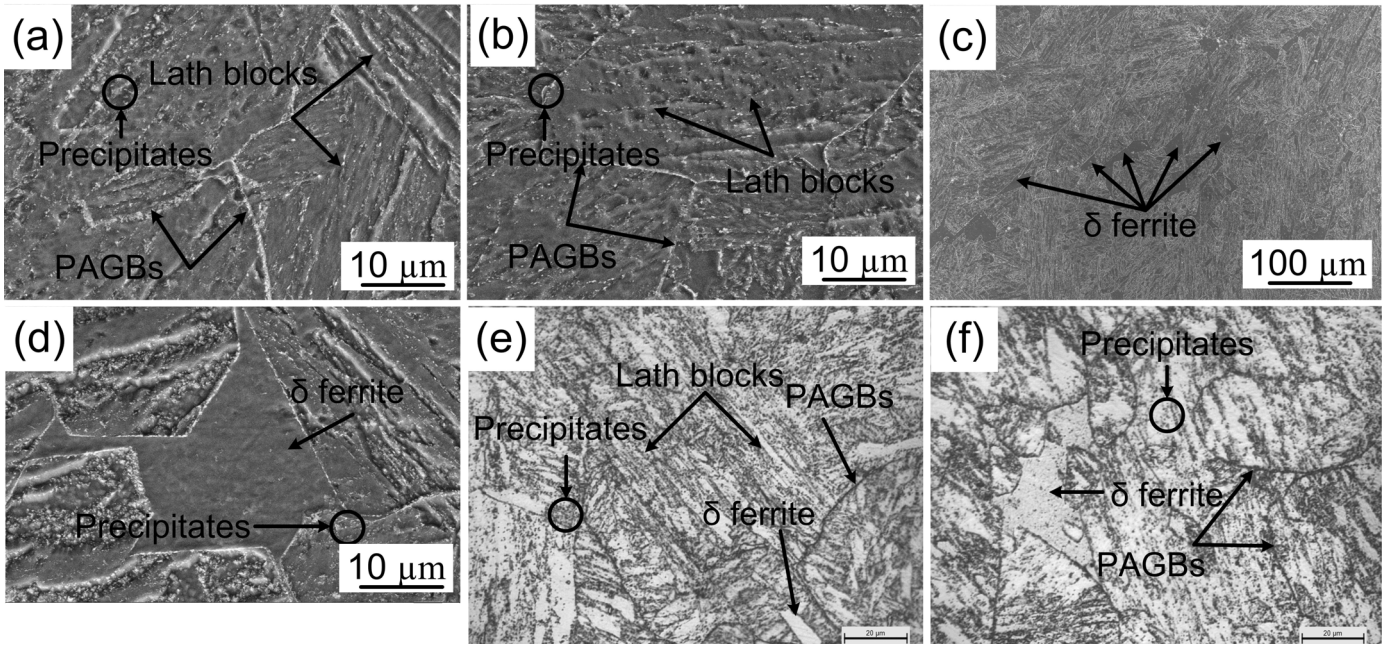


Fig. 5. SEM micrograph of the fusion zone after the PWHT for P91 steel welded joint (a) and (b), respectively; (c) and (d) P92 steel welded joint, respectively; optical micrograph of fusion zone (e) P91 steel welded joint, (f) P92 steel welded joint

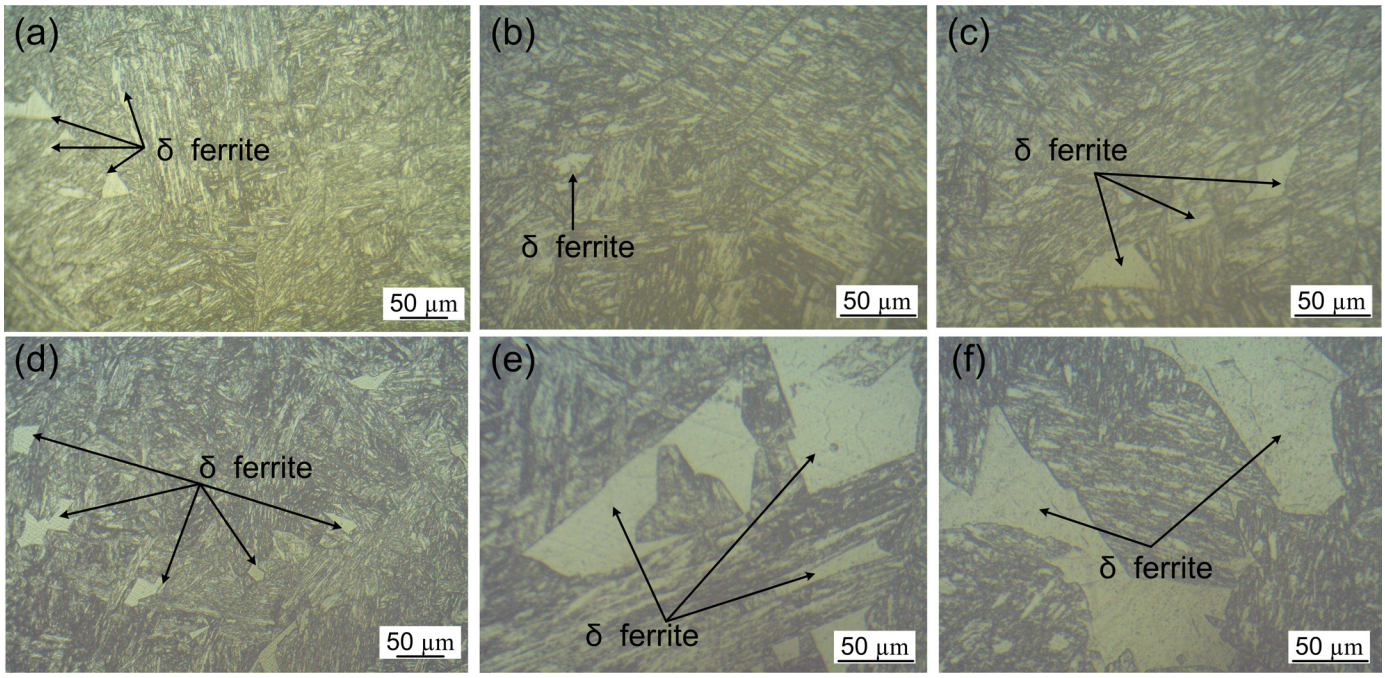


Fig. 6. Optical micrograph of the fusion zone after the PWHT for P91 steel welded joint (a), (b), and (c), respectively; fusion zone after the PWHT for P92 steel welded joint (d), (e), and (f), respectively

coarse precipitates remain undissolved and get coarsened during the normalizing process and still remain in the microstructure after the tempering treatment. In FZ of P92 welded joint, the columnar lath morphology gets restored after the PWNT treatment, however, in P91 FZ, it shows the formation of equiaxed tempered laths. To confirm the formation of coarse precipitates along the intergranular region, SEM micrograph has been taken and discussed below.

The micrograph of FG for both the welded joint is shown in Fig. 8. The Fig. 8a shows the equiaxed laths with coarse $M_{23}C_6$ precipitates along the intergranular region or PAGBs for FZ of P91 welded joint. The higher magnification micrograph shows the distribution and morphology of precipitates present in the transgranular region (Fig. 8b). The surrounding of coarse precipitates having a size in the order of the 250-350 nm is clearly seen from the Fig. 8b. The presence of coarse precipitates might act as the cavity during the prolonged creep exposure as a result of their brittle nature. For P92 welded joint, typical columnar

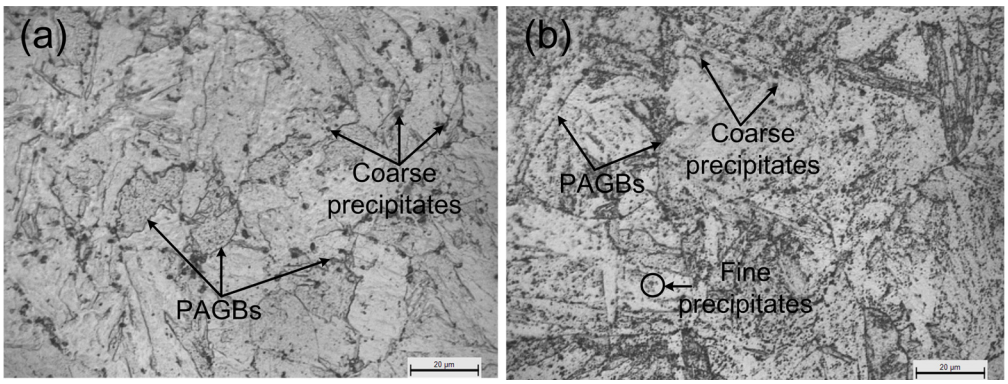


Fig. 7. Optical micrograph of fusion zone after the PWNT treatment for (a) P91 welded joint, (b) P92 steel welded joint

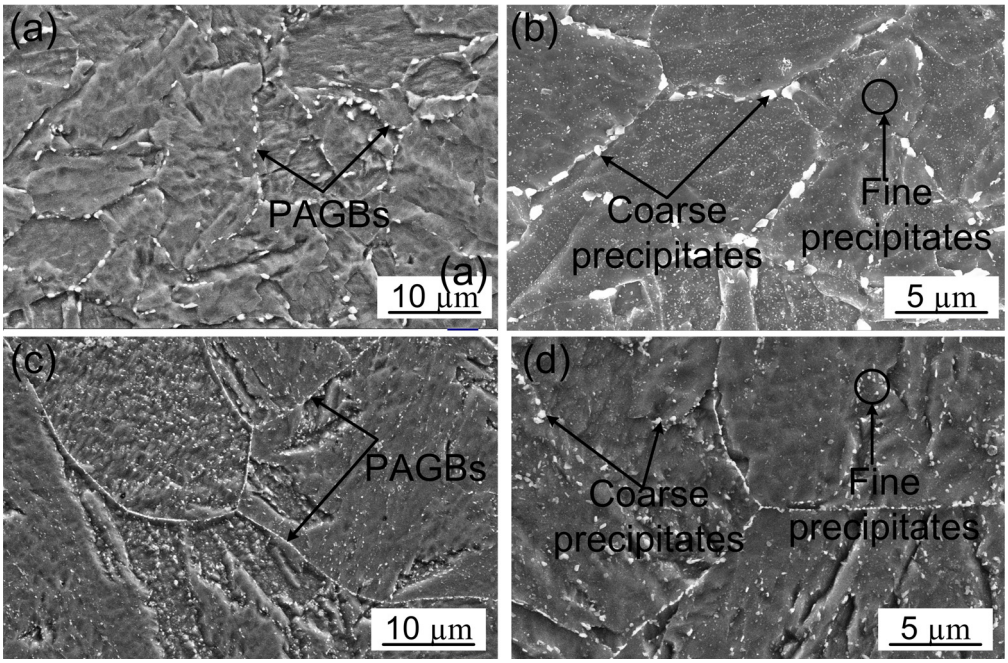


Fig. 8. Micrograph of fusion zone after the PWNT treatment for (a) P91 welded joint, (b) P92 steel welded joint

lath morphology is observed as a result of the PWNT treatment. The size of $M_{23}C_6$ precipitates is observed to be much lower for P92 welded joint, as shown in Fig. 8d. However, size of transgranular precipitates is observed higher for the FZ of P92 welded joint as compared to P91 welded joint. The size of intergranular precipitates is measured in the range of 100-200 nm for the FZ of P92 welded joint. The fine precipitates present along the intergranular region might be helpful to enhance the creep strength of the welded joint. The most important things that resulted from the PWNT treatment is the dissolution of the soft $\delta$ ferrite. In P92 FZ, the PAGs are also observed to be coarse as compared to FZ of P91.

### 3.3. Microhardness

The hardness of the FZ was measured for both the welded joint and depicted in Table 3. The hardness was measured at a load of 500 g for a dwell time of 10 s. In as-welded condition, FZ reveals the presence of untempered lath martensite for both the welded joint [24,25]. The hardness of the P91 FZ was measured 430±17 while for the P92 FZ, it was 412±35. The hardness of the untempered lath martensite generally reported in the range of 400-480 HV [25]. However, in P91 and P92 FZ, a great variation in hardness was noticed. In FZ of P91, the variation in hardness is attributed to the presence of few amounts of the soft $\delta$ ferrite. In P92 FZ, the great variation in hardness is attributed to the presence of higher number density of the $\delta$ ferrite in the FZ as shown in the micrograph. The hardness of the soft $\delta$ ferrite was measured in the range of 179-249 HV for the P92 welded joint while for P91 welded joint it was measured in the range of 300-350 HV as a result of the small zone. The PWDT treatment contributes the significant reduction in the hardness of the FZ for both the welded joint as a result of the softening of the martensite and reduction in solid solution hardening. The reduction in solid solution hardening is attributed to the evolution of the new precipitates. However, the hardness variation still remains due to the presence of the $\delta$ ferrite. The PWNT

treatment results in negligible variation in hardness for both the FZ as a result of the dissolution of the precipitates. The hardness was measured 211±6 HV and 223±8 HV for the FZ of P91 and P92 steel welds, respectively. The lower hardness in the FZ of P91 welded joint after the PWNT treatment is attributed to the coarse $M_{23}C_6$ precipitates and over-tempering of the martensite.

TABLE 3

Microhardness of the FZ for both P91 and P92 welded joint

| Heat treatment of the welds joint | Microhardness of weld fusion zone (HV) | |
|---|---|---|
| | P91 FZ | P92 FZ |
| As-welded | 430±17 | 412±35 |
| PWDT | 272±13 | 248±25 |
| PWNT | 211±6 | 223±8 |

## 4. Conclusions

The microstructure evolution in fusion zone (FZ) of P91 and P92 steel TIG welded joint have been studied in different heat treatment condition (as-welded, PWDT and PWNT). In as-welded condition, P92 steel welded joint showed a higher propensity to the formation of $\delta$ ferrite as a result of high weight percentage of ferrite stabilizer. In P91 steel welded joint the fewer amount of $\delta$ ferrite is observed. The $\delta$ ferrite present in FZ has observed a negligible response to PWDT. However, PWDT led to the softening of martensite. The PWNT treatment resulted in homogeneous microstructure formation. The $\delta$ ferrite also gets dissolved after the PWNT and it did not observe after the PWNT treatment for both P91 and P92 welded joint. In as-welded condition, the $\delta$ ferrite present in FZ led to a great variation in microhardness due to its soft nature. In P91 hardness variation was less as compared to P92 welded joint as a result of less number density of the $\delta$ ferrite. The drastic reduction in FZ was measured after the PWDT treatment, however, the variation in hardness still remain due to the negligible response of $\delta$ ferrite to PWDT. The acceptable microstructure and microhardness are observed for the PWNT treatment for both P91 and P92 steel welded joints.

## REFERENCES


[1] C.G. Panait, W. Bendick, A. Fuchsmann, A.F. Gourgues-Lorenzon, J. Besson, International Journal of Pressure Vessels and Piping **87**, 326 (2010).

[2] C. Pandey, M.M. Mahapatra, P. Kumar, N. Saini, Journal of Nuclear Materials **498**, 176 (2018).

[3] R.L. Klueh, International Materials Reviews **50**, 287 (2005).

[4] D.J. Abson, J.S. Rothwell, International Materials Reviews **58**, 437 (2013).

[5] N. Saini, C. Pandey, M.M. Mahapatra, Materials Science and Engineering A **688**, 250 (2017).

[6] C. Pandey, M.M. Mahapatra, P. Kumar, R.S. Vidyrathy, A. Srivastava, Materials Science and Engineering A **695**, 291 (2017).

[7] C. Pandey, M. Mohan Mahapatra, P. Kumar, N. Saini, Journal of Pressure Vessel Technology **140**, 1 (2018).

[8] P.J. Ennis, A.Z. Lipiec, O. Wachter, A.C. Filemonowicz, Acta Materialia **45**, 4901 (1997).

[9] L. Maddi, G.S. Deshmukh, A R. Ballal, D.R. Peshwe, R.K. Paretkar, K. Laha, M.D. Mathew, Materials Science and Engineering A **668**, 215 (2016).

[10] C. Pandey, M.M. Mahapatra, P. Kumar, N. Saini, Materials Science and Engineering A **712**, 720 (2018).

[11] C. Pandey, M.M. Mahapatra, P. Kumar, Archives of Civil and Mechanical Engineering **18**, 1000 (2018).

[12] Y. Wang, L. Li, Welding Journal **95**, 27 (2016).

[13] W. Xue, Q. Gang Pan, Y. Ren, W. Shang, H. Zeng, H. Liu, Materials Science and Engineering A **552**, 493 (2012).

[14] M. Divya, C.R. Das, S.K. Albert, S. Goyal, P. Ganesh, R. Kaul, J. Swaminathan, B.S. Murty, L.M. Kukreja, A.K. Bhaduri, Materials Science and Engineering A **613**, 148 (2014).

[15] C. Pandey, M.M. Mahapatra, P. Kumar, N. Saini, J.G. Thakre, R.S. Vidyarthy, H.K. Narang, Archives of Civil and Mechanical Engineering **18**, 713 (2018).

[16] C. Pandey, M.M. Mahapatara, P. Kumar, N. Saini, Journal of Manufacturing Processes **31**, 247 (2018).

[17] J.A. Francis, G.M.D. Cantin, W. Mazur, H.K.D.H. Bhadeshia, Science and Technology of Welding and Joining **14**, 436 (2009).

[18] C. Pandey, M.M. Mahapatra, P. Kumar, Materials Science and Engineering A **731**, 249 (2018).

[19] C. Pandey, A. Giri, M.M. Mahapatra, International Journal of Steel Structures **16**, 333 (2016).

[20] C. Pandey, M.M. Mahapatra, P. Kumar, A. Giri, Metals and Materials International **23**, 900 (2017).

[21] C. Pandey, M.M. Mahapatra, P. Kumar, N. Saini, A. Srivastava, Journal of Manufacturing Processes **28**, 220 (2017).

[22] C.R. Das, S.K. Albert, A.K. Bhaduri, B.S. Murty, Metallurgical and Materials Transactions A: Physical Metallurgy and Materials Science **44**, 2171 (2013).

[23] C. Pandey, M.M. Mahapatra, P. Kumar, N. Saini, Journal of Alloys and Compounds **743**, 332 (2018).

[24] C. Pandey, M.M. Mahapatra, Transactions of the Indian Institute of Metals **69**, 1657 (2016).

[25] C. Pandey, M.M. Mahapatra, Journal of Materials Engineering and Performance **25**, 2761 (2016).